CHAPTER 6

Effect of N52R mutation at the SPN-ARR interface on the conformational dynamics of SHANK3

Effect of N52R mutation at the SPN-ARR interface on the conformational dynamics of SHANK3

6.1. Abstract

Autism spectrum disorder (ASD) is a complex neurodevelopmental condition. The genetic basis of ASD involves numerous loci converging on neural pathways, particularly affecting excitatory synapses. SHANK3, an essential protein in the post-synaptic neurons, has been implicated in ASD, with mutations affecting its N-terminal, including the SPN domain.

This study aims to investigate the impact of the N52R mutation on SHANK3 and assess the dynamics, stability, flexibility, and compactness of the N52R mutant compared to SHANK3 WT. Molecular dynamics simulations were conducted to investigate the structural dynamics of SHANK3 WT and the N52R mutant. The simulations involved heating dynamics, density equilibrium, and production dynamics. The trajectories were analyzed for RMSD, RMSF, Rg, hydrogen bond analysis, and secondary structure.

The simulations revealed that the N52R mutant disrupts the stability and folding of SHANK3, affecting intramolecular contacts between SPN and ARR. This disruption opens up the distance between SPN and ARR domains, potentially influencing the protein's interactions with partners, including the reduction of αCaMKII affinity to the ARR domain, in contrast, higher affinity of α-Fodrin to its site on SHANK3. The altered conformation of the SPN-ARR tandem in the N52R mutant suggests a potential impact on dendritic spine shape and synaptic plasticity.

The findings shed light on the structural consequences of the N52R mutation in SHANK3, emphasizing its role in influencing intramolecular interactions and potential effects on synaptic function. Understanding these molecular dynamics contributes to unraveling the intricate relationship between genetic variations in SHANK3 and clinical traits associated with ASD. Further investigations are warranted to explore the physiological implications of these structural alterations *in vivo*.

6.2. Introduction

Autism spectrum disorder (ASD) is a neural development condition that develops in the first years of infancy, manifested by aberrations in communication, social interaction, and the presence of stereotyped behaviors [1, 2]. Numerous genetic loci have been attributed to pathomechanisms of ASD; nonetheless, they converge to a few neural pathways that are implicated in abnormal transmissions at excitatory synapses [3]. Accordingly, one of the primary mechanisms underpinning the pathophysiology of ASD has been proposed to be the disturbance of post-synaptic neuronal excitation [4]. SHANK3 is vital protein involved in the post-synaptic density. SHANK3 was extensively investigated in the PSD of neuronal cells as a scaffolding protein [5]. Mutant forms and dysregulation in SHANK3 are associated with ASD [6-8]. Remarkably, missense mutations have been pointed out as concentrated loci in the N-terminus [9]. Two mutations linked to autism, R12C and L68P, situated in the SPN region, lead to the compromised capacity of SHANK3 to interact with Rap1, inhibiting the activation of integrin [10, 11]. The experimental observations suggest that the N52R mutant exposed the ARR region, enabling posterior linking to external GFP-SPN. Besides, the N52R, which either impedes or heightens the functional role of SHANK3 to bind actin, consequently affects documented SHANK3-regulated ASD-like symptoms *in vivo* [12]. A recent study discovered that N52R disruption in the interface of SPN−ARR caused the lack of αCaMKII ligating, which emerges to be a more common outcome of SHANK3 missense variants. They theorized the physiological impact of this connection might derive from the negative regulator actions of SHANK3 on the αCaMKII signaling pathway intensely engaged in synaptic plasticity [13].

The overall aim of the stated research is to reveal further the effect of SHANK3 point mutation N52R on synapse structure, function, and plasticity. To gain insight into the complicated relationship of the clinical traits and genetic variations of SHANK3 N52R mutant compared to SHANK3 wild type (WT) and ASD pathogenesis. SHANK3 WT and SHANK3 N52R mutant were simulated using MD simulation to assess the stability of both structures with regard to the protein equilibrium, flexibility, compactness, and intramolecular hydrogen bond interactions between SPN and ARR domains. Consequently, the characterization of the SHANK3 N52R mutant, as detailed above, serves as a crucial baseline for evaluating the dynamic structural impacts of ASD-

related mutations in SHANK3, as well as can be potent parameters in elucidating the mechanisms affected by ASD-associated mutants. Additionally, evaluation of the potential effects of deleterious mutation on the protein binding sites that affect neuronal transaction and synaptic plasticity.

6.3. Materials and Methods

6.3.1. Construction of initial structures

6.3.1.1. Acquiration of SHANK3 protein

The SH3 and multiple ankyrin repeat domains 3 structure, PDB ID 5G4X [11], was acquired from RCSB Protein Data Bank [14] and was utilized for molecular dynamics simulation.

6.3.1.2. Constructing the mutant N52R SHANK3

The primary configuration of the SHANK3 N52R mutant was produced by altering the three-dimensional configuration of the scaffold protein SHANK3 WT (PDB ID: 5G4X). The Rotamer tool of the CHIMERA program [15] was utilized to generate N52R SHANK3, where Aspargine was substituted with Arginine at nucleotide 52 in the SPN domain of SHANK3.

6.3.2. Setup for Molecular Dynamics simulations

SHANK3 WT and SHANK3 N52R mutant systems were constructed for the MD simulation utilizing ff99SBildn as a force field parameter in the Leap module of the AMBER 14 software package [16]. An obvious TIP3P water model [17] was applied as a solvent to explicitly stated SHANK3 WT and SHANK3 N52R mutant systems independently utilizing a buffer dimension of 10 Å in a cubic box periodic. The WT and N52R structures have been balanced by placing adequate values of neutralizing ions and, afterward, undergoing a reduction of energy to eliminate the London dispersion force.

The molecular dynamics simulation adheres to a consistent method comprising thermal dynamics followed by density, equilibrium, and production dynamics. Initial structures were energy-minimized for further Molecular Dynamics procedures. The gradual heating of structures from 0 to 300 K occurred under a steady volume (NVT) situation, followed by the density approach. Equilibration was accomplished under NPT conditions (300 K

and 1 atm pressure) for one nanosecond. Visualization and analysis of energy, temperature, and pressure were undertaken to ensure correct equilibration. Subsequently, a 200 ns MD production run for stabilized structures using the PME algorithm [18, 19] with a time phase of 2 fs. A threshold of 8 Å addressed nonbonding connections, whereas electrostatic forces were managed using the PME technique. The SHAKE algorithm restricted all bonds [19], while temperature and pressure were maintained stationary via the Berendsen weak coupling algorithm over the simulation [20]. Snapshots were taken through the trajectory at intervals of 10 ps for future investigations of each structure.

The PTRAJ and CPPTRAJ modules of AmberTools 14 were applied to analyze molecular dynamics trajectories of both the WT and SHANK3 N52R mutant of AmberTools 14. To evaluate the convergent behavior of our structures, the RMSDs for WT and SHANK3 N52R mutant have been analyzed, wherein the initial MD system was employed as the template for analysis, and the point of convergence of simulation system for both WT and SHANK3 N52R mutant structures was further examined using the block average root-mean-square distance approach [21]. In the current procedure, the MD tracks of WT and SHANK3 N52R mutant were segmented into consecutive blocks following alignment with the corresponding reference average structure. Subsequently, the average structure for each block and the RMSD between each average structure were calculated. The average RMSD scores and SD of RMSD scores at each block size were then presented as an indicator of block size.

Besides that, The two structures underwent Radius Gyration, hydrophobic interactions, and intramolecular distance analysis. The analysis of intra-molecular hydrogen bonds was performed for WT and SHANK3 N52R mutant according to the potential donors (HD) and acceptors (HA) of the protons. UCSF Chimera software [15] was utilized to depict the 3D structure of each system. The xmgrace plotting tools were applied to generate the plots. The precision of the NPT algorithm, along with the monitoring of pressure, temperature, kinetic energy, total energy, and potential energy, was systematically validated over the course of the simulation time for both the WT and SHANK3 N52R mutant systems.

6.3.3. Docking between the two structures and αCaMKII analysis

The docking between the two structures, WT protein and SHANK3 N52R mutant with αCaMKII and α-Fodrin protein partners, was conducted using a ClusPro (protein-protein docking) server, and the results were analyzed through the PDBsum server.

6.4. Results

6.4.1. The root mean square deviation (RMSD)

RMSD analysis was conducted on a 200 ns simulation encompassing the SHANK3 WT protein and SHANK3 N52R mutant, providing insights into their respective conformational dynamics. The SHANK3 WT protein exhibited a gradual increase in RMSD, displaying initial fluctuations, followed by a prominent switch around 85 ns, until stabilization at the end of the simulation (**Figure 6.1A)**. Conversely, the SHANK3 N52R mutant exhibited an abrupt increase in RMSD, followed by fluctuations and another impulse at 4.2 Å (**Figure 6.1C)**. These results suggest that the SHANK3 WT could be slightly stable compared to the SHANK3 N52R mutant, which might have high structure flexibility. To discern the domain contributing to these conformational changes, RMSD plots were accomplished independently for the SPN, ARR, and Linker regions. Indeed, RMSD traces confined to the SPN and ARR domains were observed for the entire SHANK3 WT protein, as exhibited in (**Figure 6.1B)**. In contrast, in the SHANK3 N52R mutant, the SPN domain peak was distinct high from 100 ns and over simulation time, indicating that the SPN domain may involved in structural changes (**Figure 6.1D)**.

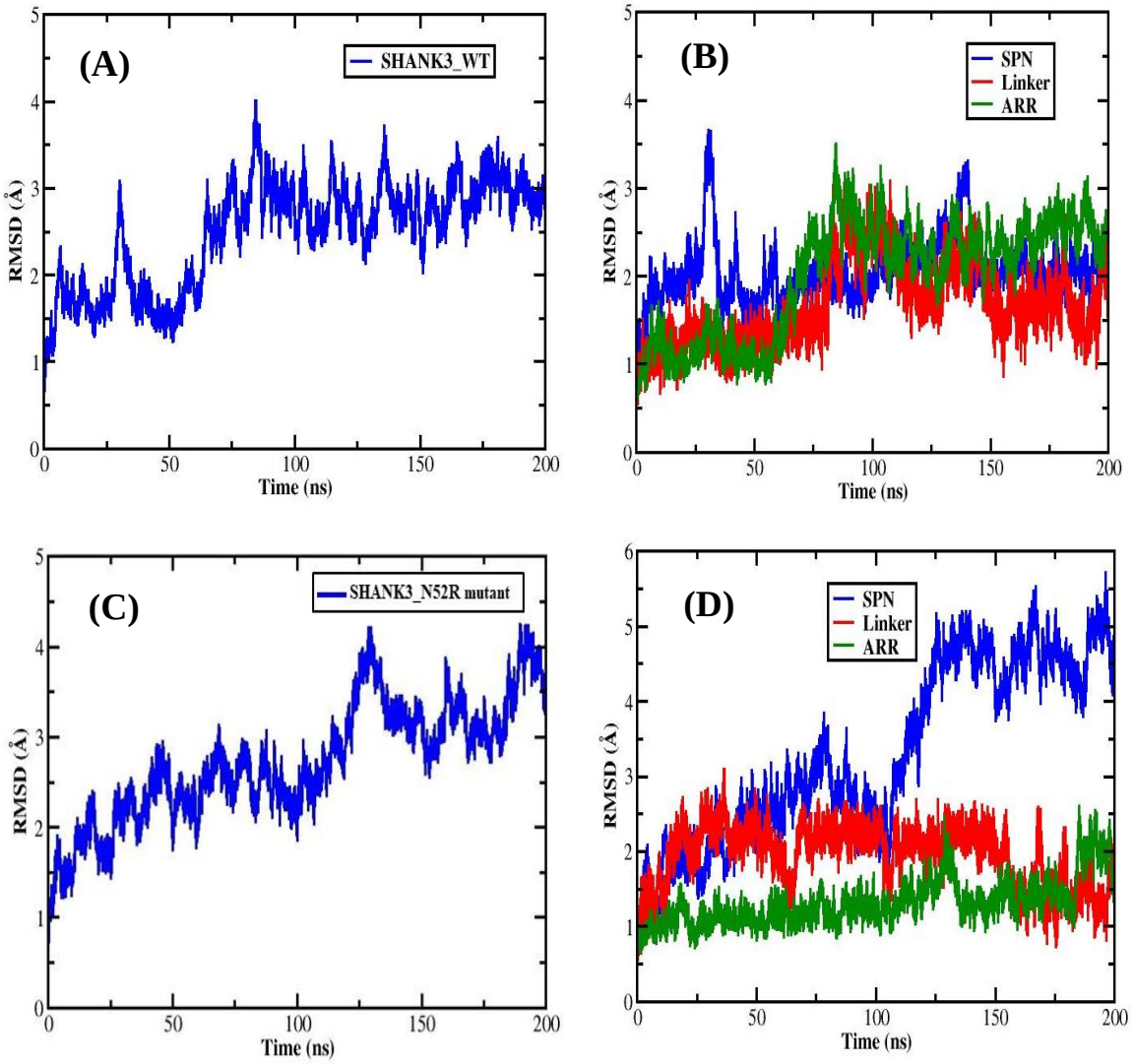

Figure 6.1 *The MD simulation analysis RMSD plot for (**A**) SHANK3 WT, (**B**) Three domains of SHANK3 WT, (**C**) SHANK3 N52R mutant, (**D**) Three domains of SHANK3 N52R mutant. The RMSD values exhibit in Angstrom are shown on the y-axis, while the x-axis exhibits the time.*

6.4.2. The root mean square Fluctuation (RMSF)

RMSF study of Cα atoms disclosed increased conformational flexibility for the SHANK3 N52R mutant (**Figure 6.2C**) compared to the SHANK3 WT protein (**Figure 6.2A**) with fluctuation around the mutation point. Notably, the flexibility of amino acid residues aligning with the SHANK3 SPN domain in the N52R mutant (**Figure 6.2D**) was found to be higher than in the SHANK3 WT protein (**Figure 6.2B**). The SPN domain with high RMSF values might be functionally important. The influence of the SHANK3

N52R mutant on SHANK3 folding has been pursued via the assessment of the Rg indicator.

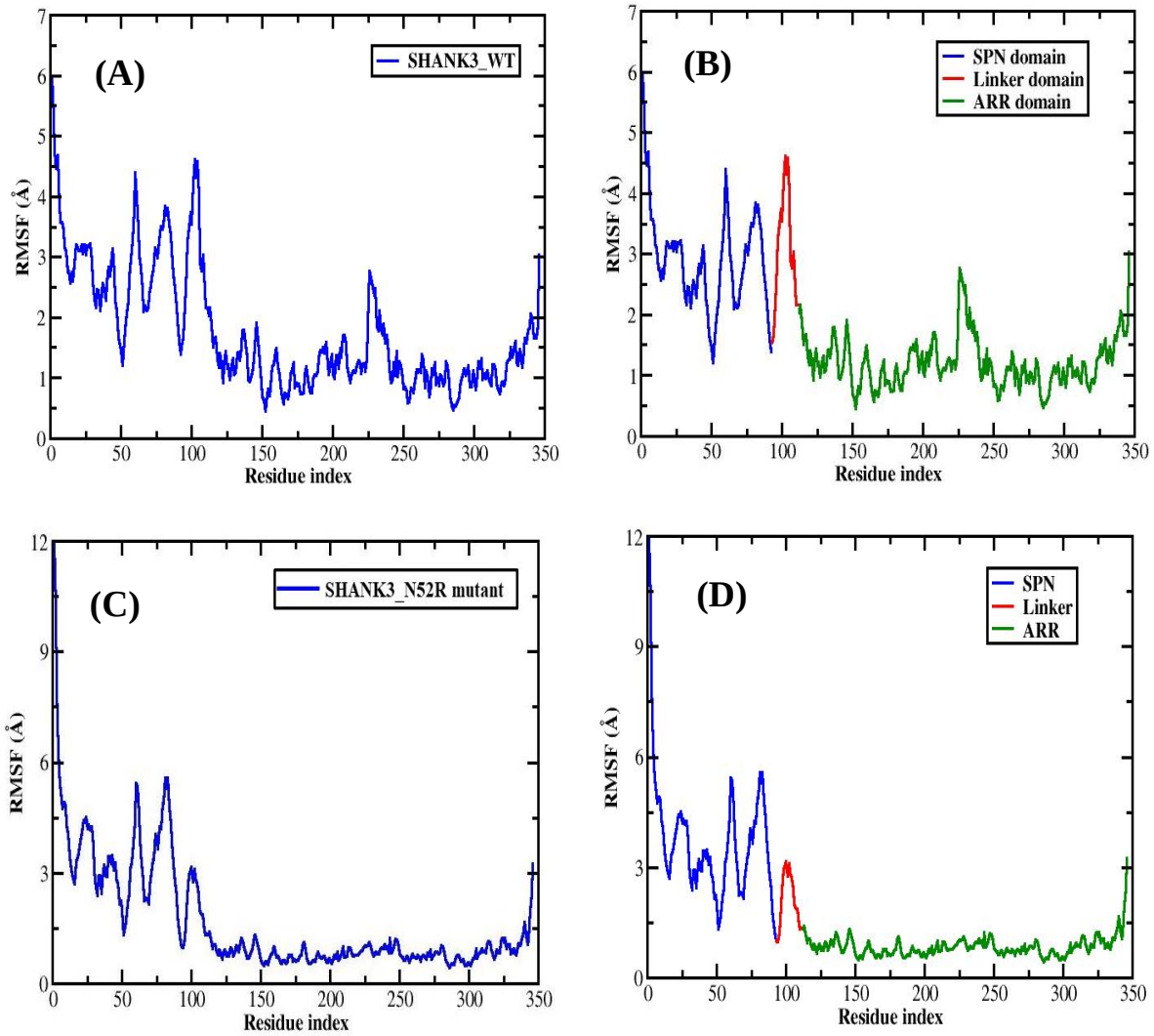

Figure 6.2 *The RMSF analysis plots (**A**) SHANK3 WT, (**B**) Three domains of SHANK3 WT, (**C**) SHANK3 N52R mutant, and (**D**) Three domains of SHANK3 N52R mutant.*

6.4.3. The radius of gyration (Rg) analysis

The Rg is a frequently employed metric for assessing the spatial distribution of atoms within a specific biological molecule, measured from the principal centre of gravity. The radius of gyration functions as a determinant of the protein's packedness and folded structure. From the Rg plot, the SHANK3 WT protein over time of simulation 200 ns revealed decreased values (**Figure 6.3A)** compared to the SHANK3 N52R mutant (**Figure 6.3B)**. An increase in the Rg of the SHANK3 N52R mutant refers to less compactness and an unfolded state.

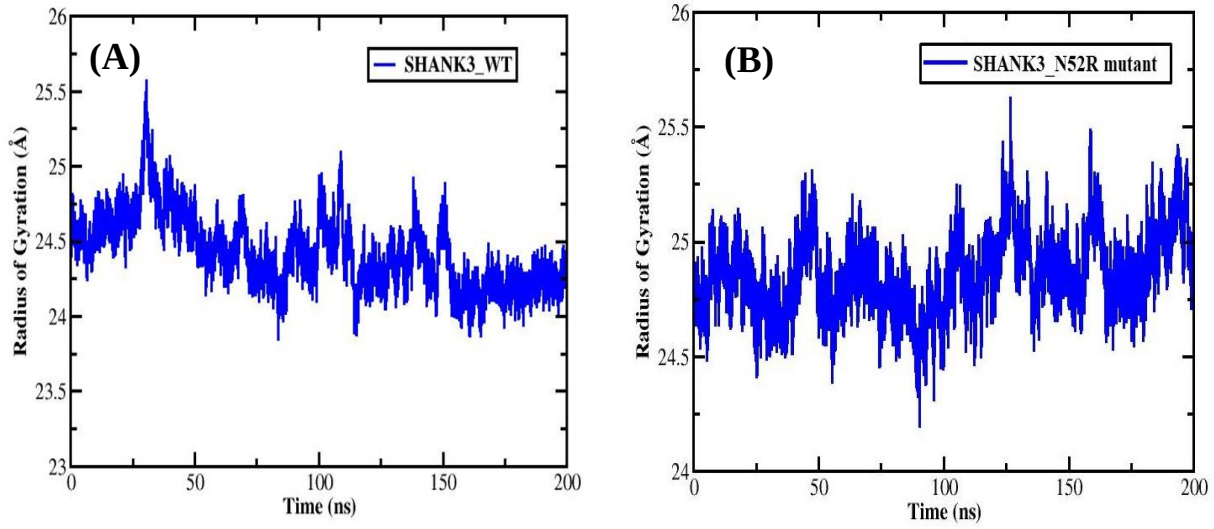

Figure 6.3 *The radius of gyration analysis (**A**) SHANK3 WT protein, (**B**) SHANK3 N52R mutant. The x-axis depicts the time ns, while the y-axis depicts the Radius gyration.*

6.4.4. The distance between SPN and ARR domains

The centre of mass distance between the SPN and ARR regions of both the SHANK3 WT protein and SHANK3 N52R mutant were analyzed as an indicator of simulation time. The length between SPN and ARR in WT protein increased at the start of the simulation, and sudden depletion was observed in (**Figure 6.4A)**. On the contrary, the N52R mutant revealed values that tend to increase over time, suggesting that the SHANK3 N52R mutant might open up the SPN-ARR fold (**Figure 6.4B)**. Earlier research indicated that intramolecular interaction prevents α-Fodrin from accessing its location on the ARR domain in SHANK3 WT [22]. However, our findings demonstrated that the SHANK3 N52R mutant increased the distance SPN-ARR domains, so the SHANK3 N52R mutant might open the conformation and facilitate α-Fodrin binding, as illustrated in (**Table 5.3** previously, and **Table 6.1**) SHANK3 N52R mutant showed higher interaction bonds than SHANK3 WT protein.

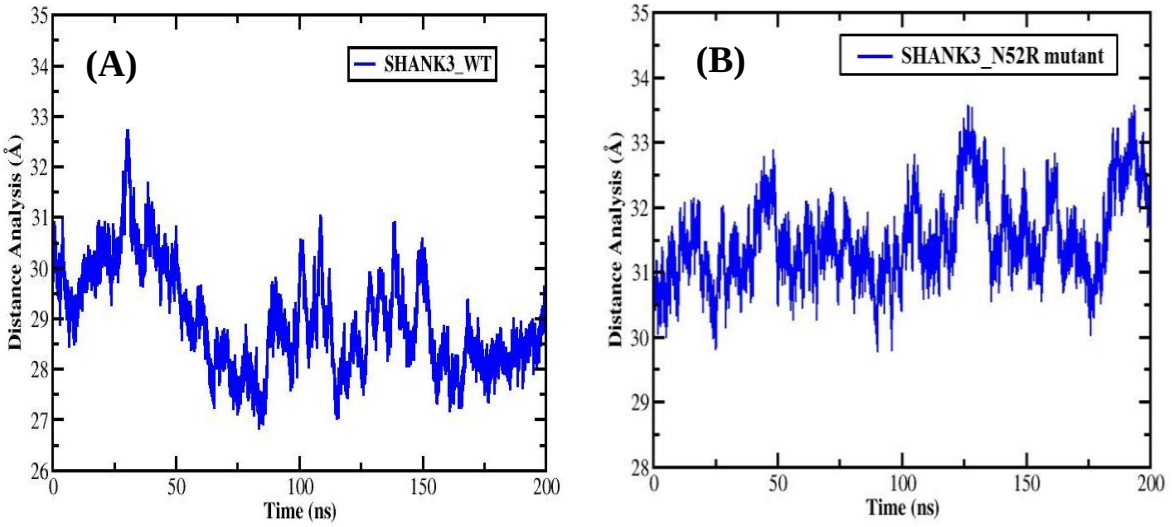

Figure. 6.4 *The distance between SPN and ARR domains analysis, (**A**) SHANK3 WT protein, (**B**) SHANK3 N52R mutant.*

Table 6.1 The interface statistics in the SHANK3 N52R mutant α-Fodrin

Chain	No. of interface residues	Interface area (A^2)	No. of salt bridges	No. of disulphide bonds	No. of hydrogen bonds	No. of non-bonded contacts
A (SHANK3 N52R)	12	664	2	-	5	112
B (α-Fodrin)	11	689				

6.4.5. Intra-molecular hydrogen bond analysis

The number of intra-molecular H-bonds was estimated to determine the vicinity of all atomic connections among the SHANK3 WT protein and in the SHANK3 N52R mutant. Intramolecular hydrogen bond interactions are substantial indicators of SHANK3 WT protein structural packedness among the different portions of SHANK3 WT protein and N52R mutant. The findings indicated a difference between the SHANK3 WT protein and the SHANK3 N52R form in (**Figures 6.5A** and **6.6A**). Similarly, the SPN and ARR domains showed no essential differences in the SHANK3 WT protein and SHANK3 N52R mutant (**Figures 6.5B** and **6.6B**), and as exhibited in (**Figures 6.5D** and **6.6D** for the ARR domain), similarly for Linker domain (**Figures 6.5C** and **6.6C**).

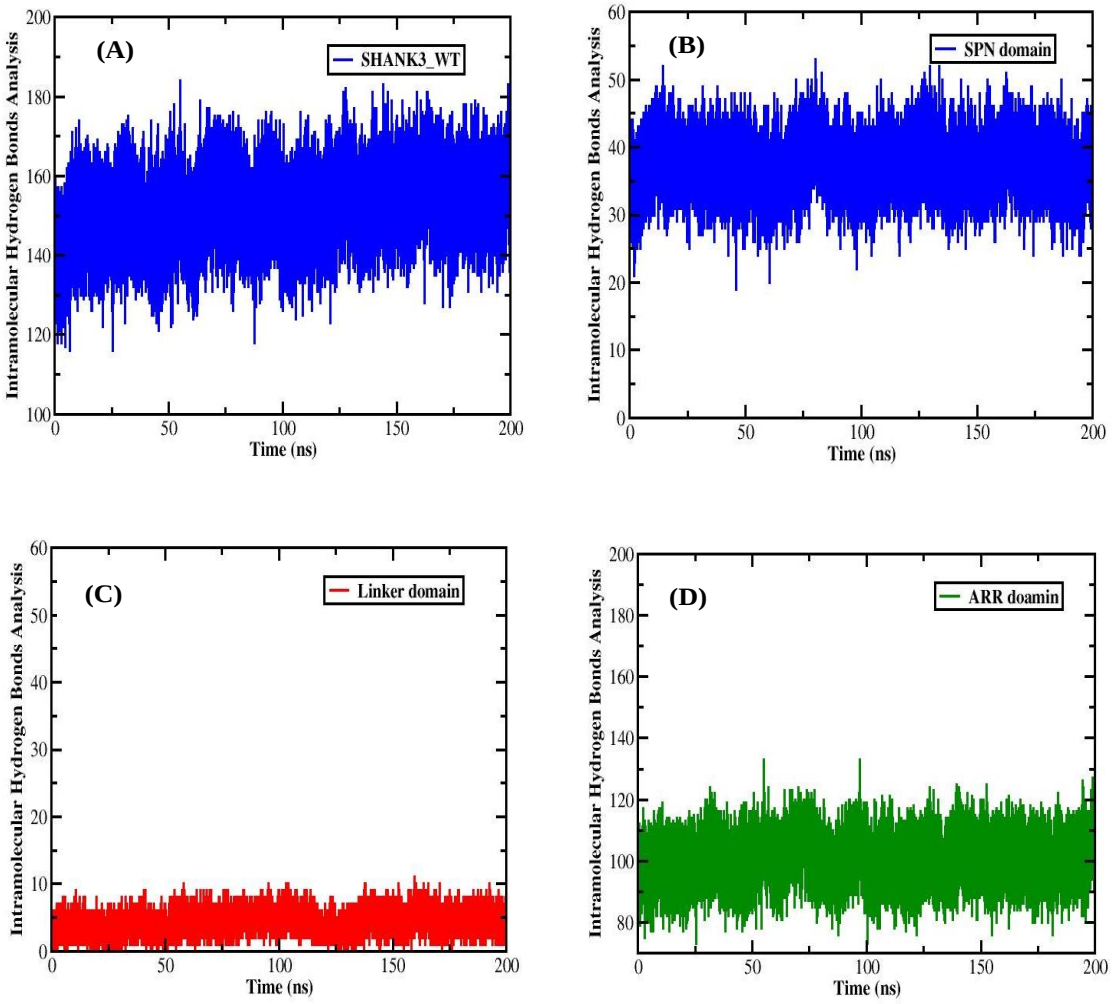

Figure 6.5 *The intramolecular hydrogen bonds analysis, (**A**) SHANK3 WT protein, (**B**) SPN domain of SHANK3 WT, (**C**) Linker domain of SHANK3 WT, (**D**) ARR domain of SHANK3 WT.*

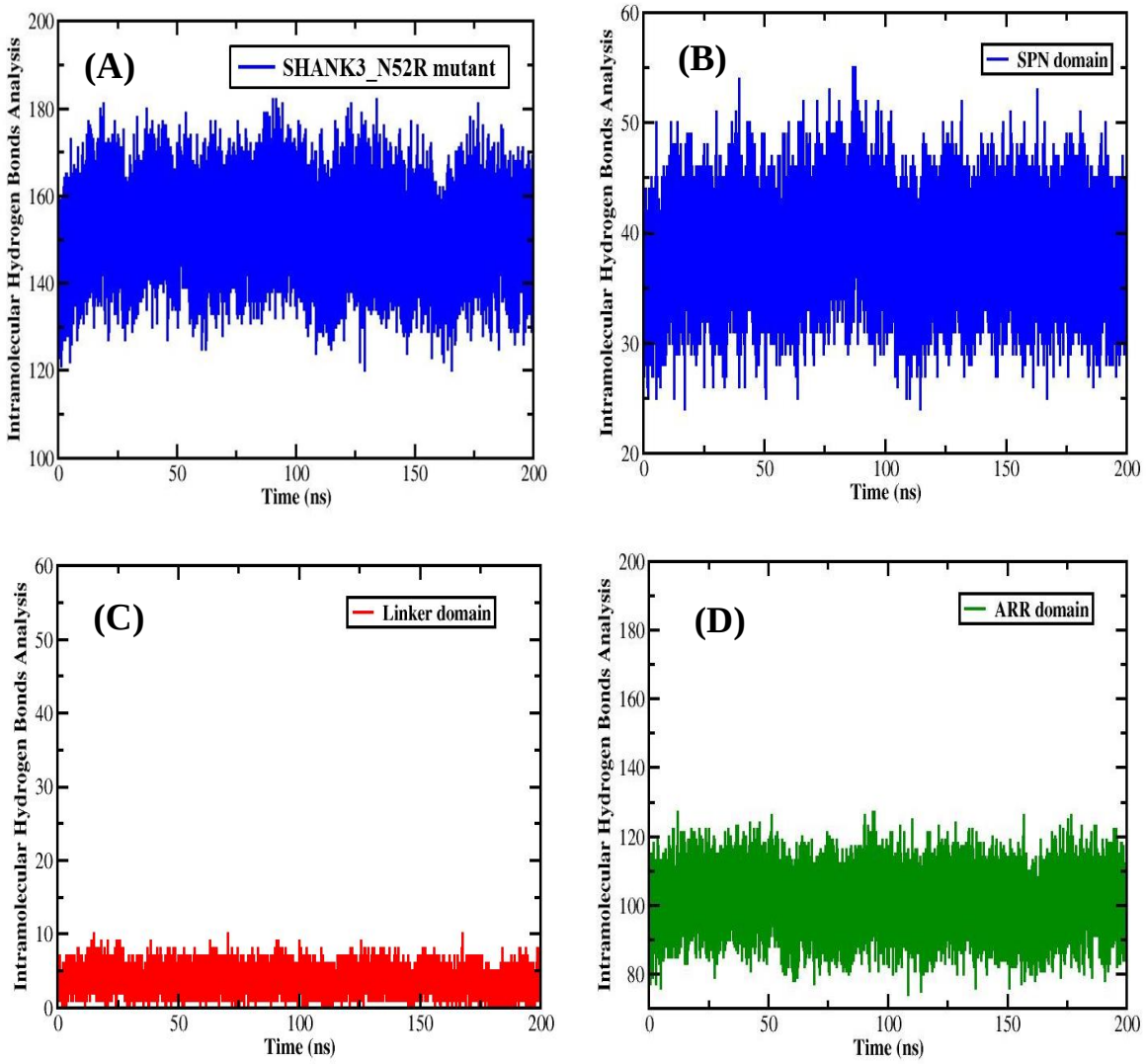

Figure 6.6 *The intramolecular hydrogen bonds analysis, (**A**) SHANK3 N52R mutant, (**B**) SPN domain of SHANK3 N52R, (**C**) Linker domain of SHANK3 N52R, (**D**) ARR domain of SHANK3 N52R.*

6.4.6. Hydrogen bond analysis

The SHANK3 WT and the SHANK3 N52R mutant were examined employing 200 ns of simulation to demonstrate the specialization of the interaction, which is a crucial feature of molecular recognition. In the case of SHANK3 WT protein and SHANK3 N52R mutant, we have considered the residues aa1-92 for the SPN domain and residues aa112-346 for the ARR domain. The findings revealed a higher average number of H-bonds between SPN-ARR domains in the SHANK3 WT (**Figure 6.7A)** than the SHANK3 N52R mutant **(Figure 6.7B)**, resulting in higher stability.

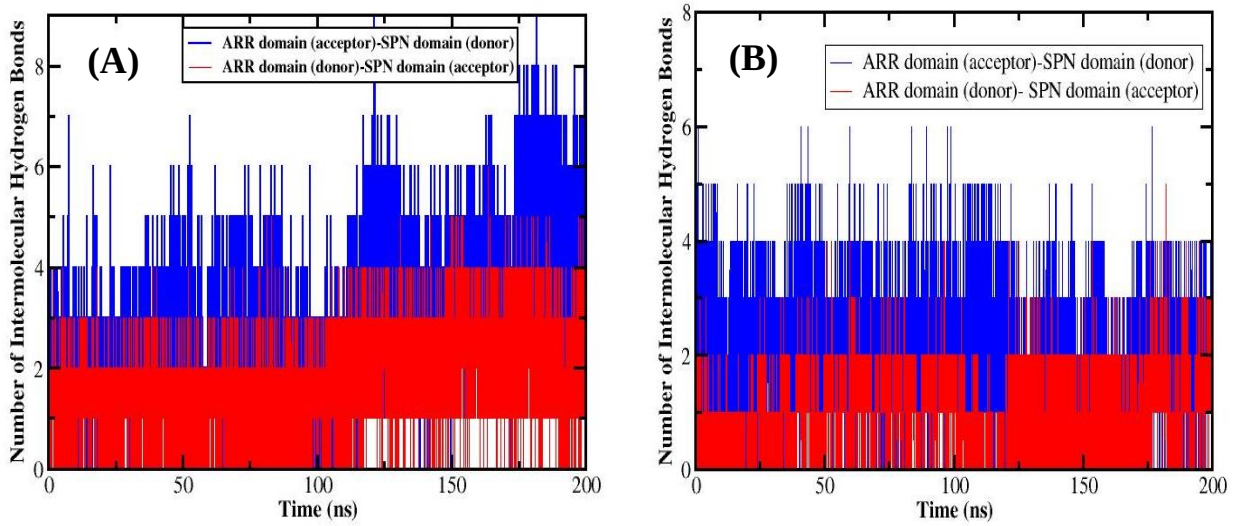

Figure 6.7 *Number of hydrogen bonds between SPN and ARR for 200 ns trajectory, (**A**) SHANK3 WT protein, (**B**) SHANK3 N52R mutant.*

6.4.7. Secondary structure analysis

The two structures, SHANK3 WT protein, and SHANK3 N52R mutant were used for the secondary structure analysis utilizing the Kabsch and Sander algorithm incorporated in their DSSP program [23]. The plots of the secondary structure results have been depicted in (**Figures 6.8A-C**) for the SHANK3 WT protein as well as (**Figures 6.9A-C**) for the SHANK3 N52R mutant. The graphic displayed the secondary structure variability across each residue as an indicator of frame numbers. Besides, using YASARA software [24], the proportion content of individual secondary structures was estimated in SHANK3 WT protein (**Figures 6.8D-F**) from their respective average structure generated by 200 ns MD simulations. The findings revealed that the secondary structure transitions are higher in the SHANK3 N52R mutant than in the SHANK3 WT protein, as shown in **Table 6.2**.

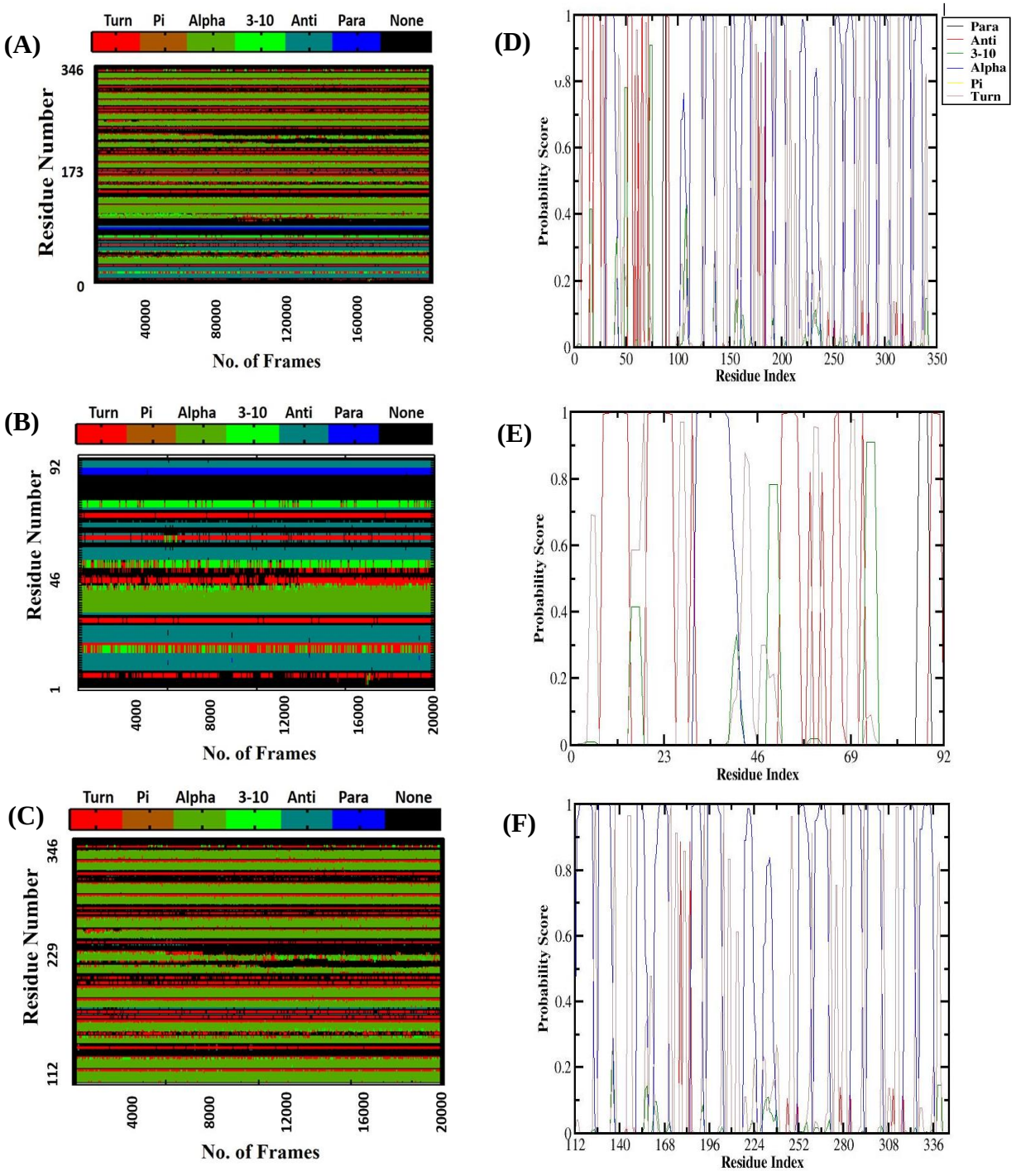

Figure 6.8 *Secondary structure analysis (**A**) SHANK3 WT, (**B**) SPN domain, (**C**) ARR domain Secondary structure probability score of residue index: (**D**) SHANK3 WT, (**E**) SPN domain, (**F**) ARR domain.*

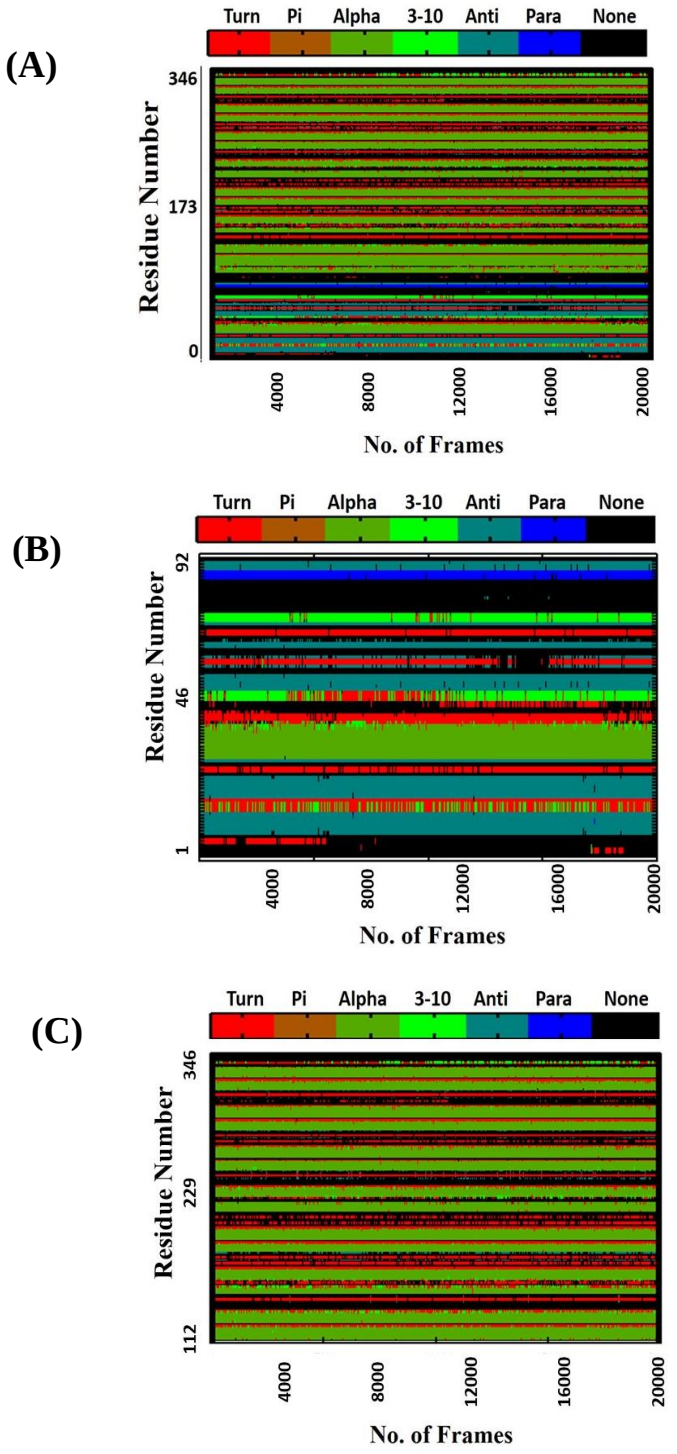

Figure 6.9 *The Secondary structure analysis for (**A**) SHANK3 N52R mutant, (**B**) SPN domain of SHANK3 N52R, (**C**) ARR domain of SHANK3 N52R.*

Table 6.2 Secondary structure content in SHANK3 WT protein and SHANK3 N52R mutant.

COMPLEX	α-helix %	β-sheet %	turn %	Coil %
SHANK3 WT	40.8	6.9	17.3	35
SHANK3 N52R MUTANT	**45.1**	9	16.2	29

6.4.8. Docking between the two structures and αCaMKII

The interactions between the SHANK3 WT protein and αCaMKII were higher, as shown in (**Figures 6.10A** and **6.11A** as well as **Table 6.3**) than those observed in the SHANK3 N52R mutant, as depicted in (**Figures 6.10B** and **6.11B** as well as **Table 6.4**).

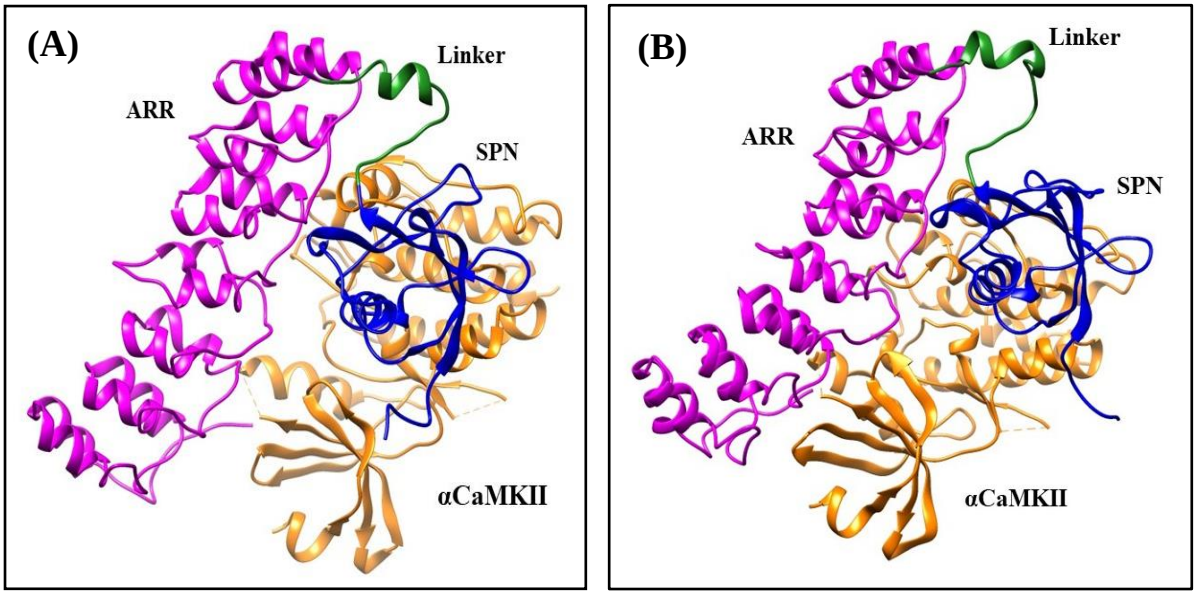

Figure 6.10 *The docking interaction between* ***(A)*** *SHANK3 WT protein and αCaMKII,* ***(B)*** *SHANK3 N52R mutant and αCaMKII.*

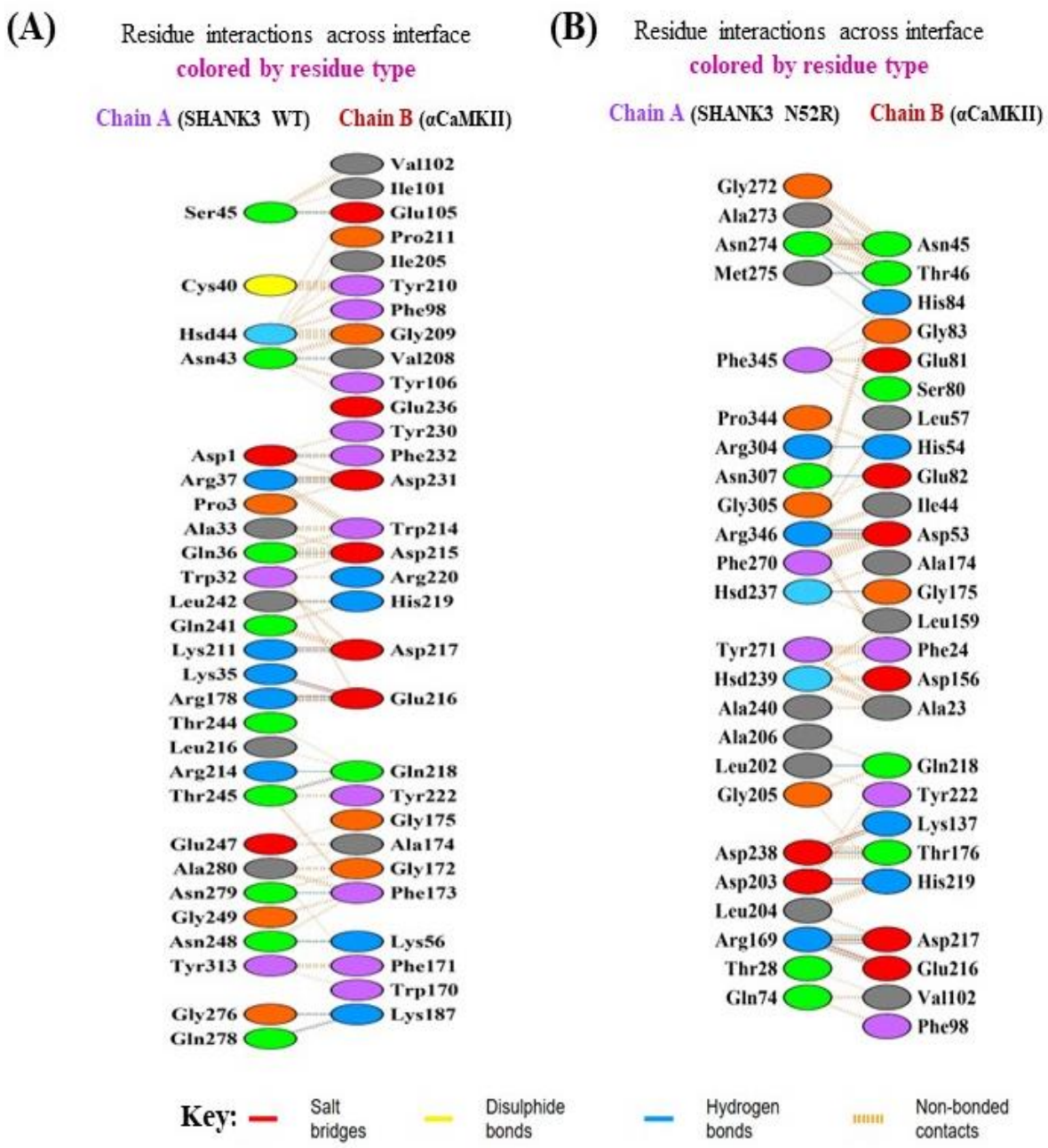

Figure 6.11 *The interactions between* ***(A)*** *SHANK3 WT protein with αCaMKII and* ***(B)*** *SHANK3 N52R mutant with αCaMKII.*

Table 6.3 The interface statistics in SHANK3 WT protein with αCaMKII.

Chain	No. of interface residues	Interface area (A^2)	No. of salt bridges	No. of disulphide bonds	No. of hydrogen bonds	No. of non-bonded contacts
A (SHANK3 WT)	27	1476	4	-	15	202
B (αCaMKII)	30	1448				

Table 6.4 The interface statistics in the SHANK3 N52R mutant with αCaMKII.

Chain	No. of interface residues	Interface area (A^2)	No. of salt bridges	No. of disulphide bonds	No. of hydrogen bonds	No. of non-bonded contacts
A (SHANK3 N52R)	24	1398	15	-	15	188
B (αCaMKII)	26	1332				

6.5. Discussion

Numerous mutations within the SHANK3 gene, encompassing nonsense, deletions, and splice site mutations, along with various missense mutations, were reported in ASD patients [6, 7, 25]. Previous reports have been shed light on the N-terminal as a functionally importance region that remains an unmet ambiguous challenge. The SPN domain was demonstrated as a highly binding-affinity region for various Ras group G-proteins, notably Rap1a and Rap1b, with two binding loci for Rap1 in the N-terminus of the SHANK3 [11, 26]. Whereas the ARR domain interacts with α-Fodrin, sharpin, and δ-catenin have been referred to as interacting partners [27, 28]. Moreover, the SPN region engages in an intramolecular interaction with the ARR domain, impeding access to specific interaction partners in the ARR region [11, 22]. In the same theme, our findings on the binding affinity indicated that the SHANK3 WT protein exhibited a greater degree of molecular interactions between the SPN and ARR domains, contributing to its overall stability and closed conformation. Several investigations have initiated the elucidation of the significance of the intramolecular interaction between

SPN and ARR [13, 25]. Our findings revealed that the SHANK3 N52R mutant might have a dramatic effect on the SPN domain as it disrupts the stability and folding of the SHANK3 protein. In addition, the SHANK3 N52R mutant could disrupt the intramolecular contacts between SPN and ARR, consequently significantly opening up the distance between SPN and ARR regions. Recent studies indicated that the linker domain linking both regions and a portion of the SPN establishes a linking surface for the αCaMKII. The occurrence of αCaMKII protein binding engaged to its inactive state, non-phosphorylated, and the SPN-ARR regions should be in a tight configuration [13, 29]. Thereby, disrupting the intramolecular between SPN and ARR regions might change the conformation of the Linker domain, causing a loss of affinity to αCaMKII. Our findings aligned with earlier studies and revealed that the docking interaction between the SHANK3 N52R mutant and αCaMKII was lower than the SHANK3 WT protein. SHANK3 appears as a suppressor regulator of the αCaMKII signaling trajectory that is significantly implicated in synaptic plasticity, which is a pivotal process underlying learning and memory [29]. Conversely, the intramolecular interaction between SPN-ARR regions inhibits access of α-Fodrin to the ARR domain. Consequently, SHANK3 N52R mutant disrupted the intramolecular interactions between SPN and ARR, which was speculated to allow for easier access of α-Fodrin to its position on ARR, which increases actin linkage and enhances integrin activation [13]. Collectively, this mutat could alter the flexibility structure of SHANK3, hindering its ability to regulate the aggregation of cytoskeletal components and causing dysregulation in signaling. Furthermore, the open conformation of the SPN-ARR tandem facilitated binding F-actin to the SPN region [12], and experimental findings revealed an increased harmony of SPN-ARR of SHANK3 N52R mutant connecting with F-actin [12]. It remains to be determined whether any type of regulated loosening of the tight SPN-ARR configuration happens *in vivo* [25]. The physiological function of SHANK3-actin interaction impacts dendritic protrusion shape in neuron cells and ASD-associated traits *in vivo* experimentation [12].

6.6. Conclusion

This study elucidates the structural repercussions of the SHANK3 N52R mutation in the SHANK3 protein, underscoring its impact on intramolecular interactions and its potential ramifications on synaptic function. Notably, the comparison between the SHANK3

N52R mutation and several mutations identified in autistic patients (e.g., R12C, L68P, Q106P, P141A) can illustrate in future studies whether point mutations located in different regions of the N-terminal, despite their proximity to the interface, can yield disparate effects on the N-terminal structure. Additionally, such comparative analyses can provide insights into the structural disparities induced by mutations and highlight the substantial impact that point mutations in critical regions of the N-terminal can exert. Besides, the MD simulation of SHANK3 N52R mutation with different analyses can serve as reliable parameters in comparison to the stability and structural conformations induced by ASD-associated mutants.

Furthermore, the insights gained into these molecular dynamics contribute to deciphering the intricate correlation between genetic variations in SHANK3 and the clinical traits associated with ASD. Subsequent investigations are essential to delve into the physiological implications of these structural alterations *in vivo*.

References

[1] Nisar, S. and Haris, M. Neuroimaging genetics approaches to identify new biomarkers for the early diagnosis of autism spectrum disorder. *Molecular psychiatry,* 1-14, 2023. https://doi.org/10.1038/s41380-023-02060-9

[2] Zeidan, J., Fombonne, E., Scorah, J., Ibrahim, A., Durkin, M. S., Saxena, S., Yusuf, A., Shih, A. and Elsabbagh, M. Global prevalence of autism: A systematic review update. *Autism research,* 15: 778-790, 2022. https://doi.org/10.1002/aur.2696

[3] Ghafouri-Fard, S., Pourtavakoli, A., Hussen, B. M., Taheri, M. and Ayatollahi, S. A. A Review on the Role of Genetic Mutations in the Autism Spectrum Disorder. *Molecular Neurobiology,* 60: 5256–5272, 2023. https://doi.org/10.1007/s12035-023-03405-9

[4] Molloy, C. J., Cooke, J., Gatford, N. J., Rivera-Olvera, A., Avazzadeh, S., Homberg, J. R., Grandjean, J., Fernandes, C., Shen, S. and Loth, E. Bridging the translational gap: what can synaptopathies tell us about autism? *Frontiers in Molecular Neuroscience,* 16: 1-20, 2023. https://doi.org/10.3389/fnmol.2023.1191323

[5] Monteiro, P. and Feng, G. SHANK proteins: roles at the synapse and in autism spectrum disorder. *Nature Reviews Neuroscience,* 18: 147-157, 2017. https://doi.org/10.1038/nrn.2016.183

[6] Satterstrom, F. K., Kosmicki, J. A., Wang, J., Breen, M. S., De Rubeis, S., An, J.-Y., Peng, M., Collins, R., Grove, J. and Klei, L. Large-scale exome sequencing study

implicates both developmental and functional changes in the neurobiology of autism. *Cell*, 180: 568-584. e23, 2020. https://doi.org/10.1016/j.cell.2019.12.036

[7] Fu, J. M., Satterstrom, F. K., Peng, M., Brand, H., Collins, R. L., Dong, S., Wamsley, B., Klei, L., Wang, L. and Hao, S. P. Rare coding variation provides insight into the genetic architecture and phenotypic context of autism. *Nature genetics*, 54: 1320-1331, 2022. https://doi.org/10.1038/s41588-022-01104-0

[8] Zhou, X., Feliciano, P., Shu, C., Wang, T., Astrovskaya, I., Hall, J. B., Obiajulu, J. U., Wright, J. R., Murali, S. C. and Xu, S. X. Integrating de novo and inherited variants in 42,607 autism cases identifies mutations in new moderate-risk genes. *Nature genetics*, 54: 1305-1319, 2022. https://doi.org/10.1038/s41588-022-01148-2

[9] Hassani Nia, F. and Kreienkamp, H.-J. Functional relevance of missense mutations affecting the N-terminal part of Shank3 found in autistic patients. *Frontiers in Molecular Neuroscience*, 11: 1-6, 2018. https://doi.org/10.3389/fnmol.2018.00268

[10] Durand, C. M., Betancur, C., Boeckers, T. M., Bockmann, J., Chaste, P., Fauchereau, F., Nygren, G., Rastam, M., Gillberg, I. C. and Anckarsäter, H. Mutations in the gene encoding the synaptic scaffolding protein SHANK3 are associated with autism spectrum disorders. *Nature genetics*, 39: 25-27, 2007. https://doi.org/10.1038/ng1933

[11] Lilja, J., Zacharchenko, T., Georgiadou, M., Jacquemet, G., Franceschi, N. D., Peuhu, E., Hamidi, H., Pouwels, J., Martens, V. and Nia, F. H. SHANK proteins limit integrin activation by directly interacting with Rap1 and R-Ras. *Nature cell biology*, 19: 292-305, 2017. https://doi.org/10.1038/ncb3487

[12] Salomaa, S. I., Miihkinen, M., Kremneva, E., Paatero, I., Lilja, J., Jacquemet, G., Vuorio, J., Antenucci, L., Kogan, K. and Nia, F. H. SHANK3 conformation regulates direct actin binding and crosstalk with Rap1 signaling. *Current Biology*, 31: 4956-4970, 2021. https://doi.org/10.1016/j.cub.2021.09.022

[13] Woike, D., Wang, E., Tibbe, D., Hassani Nia, F., Failla, A. V., Kibæk, M., Overgård, T. M., Larsen, M. J., Fagerberg, C. R. and Barsukov, I. Mutations affecting the N-terminal domains of SHANK3 point to different pathomechanisms in neurodevelopmental disorders. *Scientific Reports*, 12: 902, 2022. https://doi.org/10.1038/s41598-021-04723-5

[14] Berman, H. M., Westbrook, J., Feng, Z., Gilliland, G., Bhat, T. N., Weissig, H., Shindyalov, I. N. and Bourne, P. E. The Protein Data Bank. *Nucleic acids research*, 28: 235-242, 2000. https://doi.org/10.1093/nar/28.1.235

[15] Pettersen, E. F., Goddard, T. D., Huang, C. C., Couch, G. S., Greenblatt, D. M., Meng, E. C. and Ferrin, T. E. UCSF Chimera—a visualization system for exploratory research and analysis. *Journal of computational chemistry,* 25: 1605-1612, 2004. https://doi.org/10.1002/jcc.20084

[16] Henriques, J., Cragnell, C. and Skepo, M. Molecular dynamics simulations of intrinsically disordered proteins: force field evaluation and comparison with experiment. *Journal of chemical theory computation,* 11: 3420-3431, 2015. https://doi.org/10.1021/ct501178z

[17] Jorgensen, W. L., Chandrasekhar, J., Madura, J. D., Impey, R. W. and Klein, M. L. Comparison of simple potential functions for simulating liquid water. *The Journal of chemical physics,* 79: 926-935, 1983. https://doi.org/10.1063/1.445869

[18] Salomon-Ferrer, R., Gotz, A. W., Poole, D., Le Grand, S. and Walker, R. C. Routine microsecond molecular dynamics simulations with AMBER on GPUs. 2. Explicit solvent particle mesh Ewald. *Journal of chemical theory computation,* 9: 3878-3888, 2013. https://doi.org/10.1021/ct400314y

[19] Ryckaert, J.-P., Ciccotti, G. and Berendsen, H. J. Numerical integration of the cartesian equations of motion of a system with constraints: molecular dynamics of n-alkanes. *Journal of computational physics,* 23: 327-341, 1977. https://doi.org/10.1016/0021-9991(77)90098-5

[20] Berendsen, H. J., Postma, J. v., Van Gunsteren, W. F., DiNola, A. and Haak, J. R. Molecular dynamics with coupling to an external bath. *The Journal of chemical physics,* 81: 3684-3690, 1984. https://doi.org/10.1063/1.448118

[21] Romo, T. D. and Grossfield, A. Block covariance overlap method and convergence in molecular dynamics simulation. *Journal of Chemical Theory Computation,* 7: 2464-2472, 2011. https://doi.org/10.1021/ct2002754

[22] Mameza, M. G., Dvoretskova, E., Bamann, M., Hönck, H.-H., Güler, T., Boeckers, T. M., Schoen, M., Verpelli, C., Sala, C. and Barsukov, I. SHANK3 gene mutations associated with autism facilitate ligand binding to the Shank3 ankyrin repeat region. *Journal of Biological Chemistry,* 288: 26697-26708, 2013. https://doi.org/10.1074/jbc.M112.424747

[23] Kabsch, W. and Sander, C. Dictionary of protein secondary structure: pattern recognition of hydrogen-bonded and geometrical features. *Biopolymers: Original Research on Biomolecules,* 22: 2577-2637, 1983. https://doi.org/10.1002/bip.360221211

[24] Krieger, E., Koraimann, G. and Vriend, G. Increasing the precision of comparative models with YASARA NOVA—a self-parameterizing force field. *Proteins: Structure, Function, Bioinformatics*, 47: 393-402, 2002. https://doi.org/10.1002/prot.10104

[25] Woike, D., Tibbe, D., Hassani Nia, F., Martens, V., Wang, E., Barsukov, I. and Kreienkamp, H.-J. The Shank/ProSAP N-terminal (SPN) domain of Shank3 regulates targeting to postsynaptic sites and postsynaptic signalling. *bioRxiv*, 1-21, 2023. https://doi.org/10.1101/2023.04.28.538665

[26] Cai, Q., Hosokawa, T., Zeng, M., Hayashi, Y. and Zhang, M. Shank3 binds to and stabilizes the active form of Rap1 and HRas GTPases via Its NTD-ANK tandem with distinct mechanisms. *Structure*, 28: 290-300. e4, 2020. https://doi.org/10.1016/j.str.2019.11.018

[27] Hassani Nia, F., Woike, D., Martens, V., Klüssendorf, M., Hönck, H.-H., Harder, S. and Kreienkamp, H.-J. Targeting of δ-catenin to postsynaptic sites through interaction with the Shank3 N-terminus. *Molecular Autism*, 11: 1-17, 2020. https://doi.org/10.1186/s13229-020-00385-8

[28] Yi, F., Danko, T., Botelho, S. C., Patzke, C., Pak, C., Wernig, M. and Südhof, T. C. Autism-associated SHANK3 haploinsufficiency causes I h channelopathy in human neurons. *Science*, 352: aaf2669-1-10, 2016. https://doi.org/10.1126/science.aaf2669

[29] Cai, Q., Zeng, M., Wu, X., Wu, H., Zhan, Y., Tian, R. and Zhang, M. CaMKIIα-driven, phosphatase-checked postsynaptic plasticity via phase separation. *Cell Research*, 31: 37-51, 2021. https://doi.org/10.1038/s41422-020-00439-9